Helmholtz-Zentrum Dresden-Rossendorf (HZDR)

Balanced 20 kA DC Distributor for Magnetized Taylor Couette Systems Utilizing Thermostatic Controlled Water Valves with CO2 Adsorption Charge Sensors as Current Controller

Seilmayer, M.; Krauter, N.;

Perma-Link to Publication Repository of HZDR:

https://www.hzdr.de/publications/Publ-25902

Balanced 20 kA DC Distributor for Magnetized Taylor Couette Systems, Utilizing Thermostatic Controlled Water Valves with CO2 Adsorption Charge Sensors as Current Controller

Martin Seilmayer and Nico Krauter

Abstract—A quasi coaxial system consisting of a central current carrying copper rod and five symmetric return paths takes up to 20 kA,The installation provides a homogeneous magnetic field B_φ to a Taylor-Couette flow. One challenging part of the system is the design of the current distributor, which is supposed to divide the return current into several equally weighted lines. The individual components like the copper rods as well as all electrical contacts provide a characteristic resistance, each in the same magnitude of several $\mu\Omega$. By initial installation this will support an imbalance in the current distribution affecting the symmetry of the magnetic field. So the adjustment of current distribution becomes mandatory to ensure maximum field homogeneity. Controlling the outflow temperature of the required water cooling offers an indirect access to set the current by thermostatically operated valves with CO_2 adsorption charge in conjunction with the temperature dependent branch resistance. A numerical investigation proves that a stable current distribution can be achieved by a couple of paralleled thermal controlled heater valves with proportional characteristics. Finally, recent ironless Hall-effect current sensors help to calibrate the system so that the current homogeneity differs less than 1 % from optimal state in a wide range of currents.

I. A BRIEF INTRODUCTION

The Taylor-Couette (TC) flow experiment, concerning a rotating shear flow of a fluid between two concentric cylinders, is one of the most fundamental setups in fluid mechanics. First significant results were gained by A. H. Malloc [1], [2], M. F. Couette [3] and Lord Rayleigh [4] in the end of 19th century. Early investigations were driven by questions on the determination of fluid viscosity as well as the laws of shear and flow motion. In the case of an infinite long cylindric annulus, with inner rotation $\Omega_i = 0$ and outer $\Omega_o \neq 0$, it can be shown that the shear flow remains stable and laminar. Here, centrifugal forces push the liquid radially outward so that angular momentum increases with radius which is a sufficient condition for stability. One important parameter of viscosity measurements is flow stability, which is effected due to fast rotations. Here, secondary effects, driven by the end caps or differential rotation ($\Omega_{i,o} \neq 0$), cause non-linear flow structures in real systems. A general investigation, on this stability problem of shear flow in a cylindic geometry, was carried out two decades later by G. I. Taylor [5]. He has

Martin Seilmayer, Helmholtz-Zentrum Dresden-Rossendorf, Dresden, Germany, e-mail: m.seilmayer@hzdr.de.
Nico Krauter, —, e-mail: n.krauter@hzdr.de

theoretically and experimentally discovered the Taylor-Couette instability, which is characterized by stacked torus like vortices in the cylindrical gap.

Next to the pure hydrodynamic case, magnetized Tayor-Couette flow extends the experiment by introducing electrical conducting fluids to which magnetic fields or electric current are applied. Here, first theoretical work was done by D. H. Michel [6], S. Chandrasekhar [7] and E. P. Velikhov [8] in the mid of 20th century. It turned out that magnetic fields applied to a conducting fluid in a shear flow can lead to instability as well as to the opposite. However, magnetized shear flow gains relevance in astrophysical formation processes like evolution of accretion discs or star formation [9]. Here, several magnetohydrodynamic effects explain angular momentum transport, which cannot be expressed by pure (non-magnetic) hydrodynamic theory.

The experimental investigation on magnetized TC-flow remained open (more or less) until the theoretical work of R. Hollerbach [10] and G. Rüdiger [11], who encountered two effects observable in laboratory experiments incorporating rather slow rotation $\mathcal{O}(0.1\,\text{Hz})$ and moderate high magnetic fields generated by currents in the order of $\mathcal{O}(10\,\text{kA})$.

Experiments concerning helical magnetorotational instability (HMRI) by F. Stefani et al. [12] and azimuthal MRI by M. Seilmayer et al. [13] were carried out successfully with the PROMISE device which is shown in Figure 1. The basis of both experiments is a magnetic field B_φ in azimuthal direction which is generated by an insulated current of up to 20 kA on the central axis of the experiment. The former current support (Figure 1) forms a frame coil, with one winding, which caused a slight but significant non axis-symmetric ($m = 1$) field perturbation. Although, this imperfection did not affect the results of the HMRI, it still caused a significant stationary background flow in the AMRI experiments.

The new configuration (Figure 2) consists of a quasi coaxial setup with $n = 5$ return paths. It turns out that this small number of returns is enough to homogenize the field close to the analytical optimum in the active volume of the experiment. To understand the mechanism behind, consider Maxwell's first law

$$\oint_S \vec{B}\,\mathrm{d}s = \mu_0 \int_A \left(\vec{J} + \frac{\partial}{\partial t}\vec{D}\right)\mathrm{d}A, \qquad (1)$$

which can be interpreted in a way that only the current covered by the surface $\vec{A}$, with the closed boundary path S, contributes to the field. In other words, the field inside a coaxial
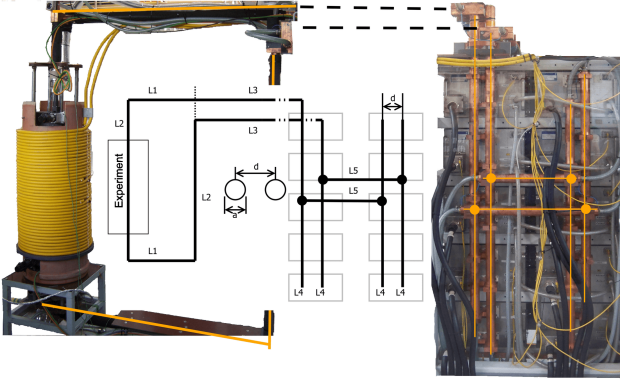
Figure 1: The PROMISE device. The previous old installation is displayed. Here the scheme of the supply rods L1 and L2 ($a = \{50, 30\}$ mm, $d > 0.17$ m) on the left side form a frame coil with one winding. This produces additional field components in the fluid, which lead to a stationary background flow structure in the frame of laboratory. The back side of the current sources and the current busbar can be seen on the right side of the picture. [1]

configuration is dominated by the central current because the field contribution from the outer currents is canceled out. At a certain distance outside the installation, all currents crossing the surface $\vec{A}$ defined by a path around everything sum to zero, so the surrounding vicinity is supposed to be field free as well.

All this works under the assumption that each return path carries the same amount of current I_{tot}/n. But, this situation is not automatically given in a design with an amperage of several kA, because resisitive components like the copper parts as well as the contact resistance have a resistivity in the same order of about $\mathcal{O}(10\,\mu\Omega)$. Due to differences in production or installation quality, all of these components differ which results in a random distribution of return current. To achieve reasonably good field homogeneity in the active volume of the experiment, current should deviate less than 5% over all return paths. Each return path, in the proposed resistive parallel network, carries up to $I_{\text{tot}} \approx 4$ kA causing $P_{\text{heat}} \approx \mathcal{O}(1\,\text{kW})$ heat flux. To prevent overheating a proper water cooling is required on each branch.

A minimal configuration of the parallel hydraulic system would require at least throttle valves which balance the coolants flow and set the outflow temperature accordingly in this way. Here, water cooling offers the option to influence a fraction of the branch resistance, if an appropriate temperature control is installed. However, the temperature dependence of the resistance is utilized to equalize the current distribution because of two reasons. First, only a minor fraction of the resistance has to be adjusted and second there are almost no (cheap) transistors available[2] to limit a current of 4 kA. With the approach to control the temperature, the design gains also advantage of a non automated (non electronic) solution, which seems in

(b) AVTA valve at the outflow position.

(c) Zoomed current sensor (black, $|I| \leq 4\,\text{kA} \pm 1\%\text{FS}$) surrounding the copper rod

(a) Whole experiment with sensor mounting in the symmetry plane.
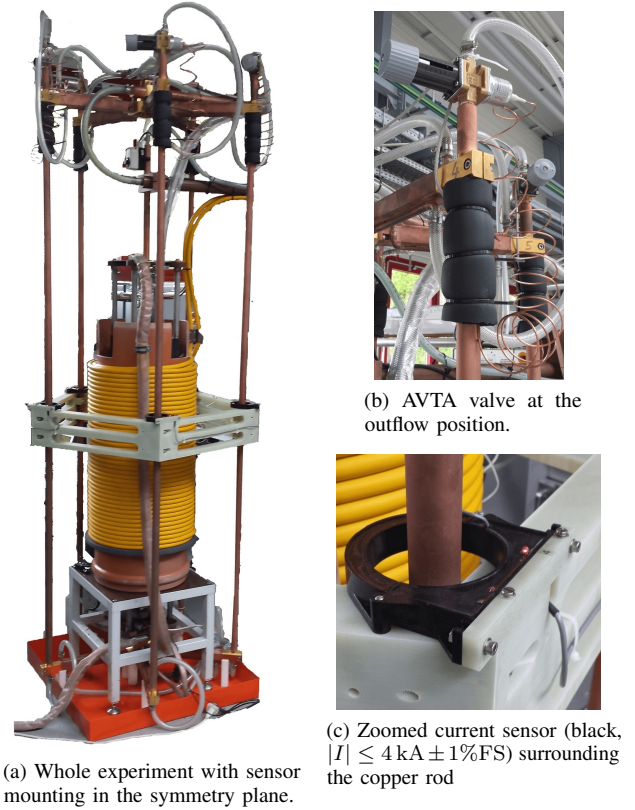
Figure 2: Setup of the new current return path. Panel (a) shows the new improved configuration. The current returns on five separate rods in a distance of about 0.8 m to the liquid. In (b) and (c) the involved sensors are displayed. The thermostatic operated AVTA valve is positioned at the outflow, whereas the sensor tip is fixed under the black insulation. Thermal paste and a form-fit junction guarantee best thermal contact between the sensor and the rod. The rod in the center of the current sensor (c) is mounted precisely in the mid point, so the geometric error might be neglectable.

comparison to be less error prone and much cheaper.

The challenge is to ensure that all five separately controlled lines still give stable performance, since a change on one branch will influence the others. For example closing a valve in one branch causes a temperature rise and lowers the current because of the higher resistance. But, at the same moment all other branches will additionally get a certain fraction of this current and heat up a bit. The same holds for the hydraulic system, where opening of one valve causes the redistribution of mass flow in all other branches which in turn leads to a change in temperature and current as well. In the end, it turns out that a simple proportional thermostatic controlled water valve is able to quell all these dependencies, even if several of such devices work in parallel. In the present design Grundfoss AVTA10 is utilized. Acting as a pressure controlled valve, the sensor tip is filled with a charge of activated carbon and CO2. The adsorption of the gas in the carbon depends on the equilibrium state of temperature and pressure. Once the temperature deviates, a pressure change follows and closes or opens the valve accordingly. A comprehensive review about

---

[1] authorized reprint from [14], Copyright 2015, Elsevier B.V.

[2] there are discontinued or outdated IGBT modules (e. g. [15]) on the market, each costing 500 €–2'000 €.

the thermophysical principle can be found in V. K. Singh et al. [16]. Figure 2b shows the installed device with the sensor tip mounted below the black insulation, where thermal paste guarantees optimal coupling.

The manual calibration of the system is supported by recent ironless Hall-effect sensors of CPCO series, measuring the current on each branch. Finally, section IV documents the commissioning run yielding an overall relative current deviation of less than 0.5%.

II. DESIGN IDEA

As seen in Figure 3 the individual sections $(1 \ldots n)$ of the electric network divide into several sub-components. From left to right, there is the contact resistance R_c which represents the connection from and to the central rod to the junction point, as seen in Figure 4b and (c). The junction point itself is made of solid copper, covered by a layer of pure gold. This ensures stable longterm performance of the contacts with respect to chemical durability (e.g. oxidation). Now, each return path includes a fraction of the temperature dependant resistance $R^*(\vartheta)$ which is determined by the exact geometry, material homogeneity and resulting current distribution in the bulk. The specific contact area and magnetic field conditions also contribute to $R^*(\vartheta)$, resulting in an individual distribution of resistivity (compare Table I and Appendix B).

Next to that, the contact R_{c2} to the radial arm follows which depends on contact pressure, surface quality (set by manufacturing process), roughness z and temperature. Furthermore, there is the copper bulk resistance R_{Cu} of the radial arm. Up to now, all this describes the series resistance components from the junction point into the radial arm. Finally, the total branch resistance

$$R_n = \underbrace{2 \cdot (R_n^* + R_{c2,n} + R_{Cu-arm,n} + R_{c3,n})}_{\text{junction and radial arm}} + \underbrace{R_{Cu-rod,n}}_{\text{vert. rod}},$$

(2)

$$\approx \underbrace{15.14\,\mu\Omega}_{\text{unknowns}} + \underbrace{67.5\,\mu\Omega}_{=f(\vartheta)}$$

consists of two parts: Twice the junction R^* and radial arm resistance including the two contacts R_c and the vertical rod resistance. In the end, the total resistance of $R_n \approx 82.6\,\mu\Omega$ splits into a well known fraction of the rod R_{Cu-rod} and a remainder which contains the unknown variables. The latter also includes the radial arm because it is not supposed to be cooled so the warming of the arm must be compensated by the vertical rod.

Table I: Resistive variation of the junction point with $R^* = (2.47 \pm 0.022)\,\mu\Omega$. The surface count n is mapped in Figure 8 to the component.

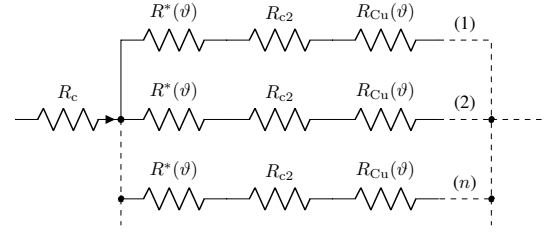| n	$R^*/\mu\Omega$
1	2.474
2	2.488
3	2.474
4	2.453
5	2.444

Figure 3: Resistive parallel network. The current is introduced left at R_c the first electrical contact. Then it splits into to individual R^*, which represent the path in the star connection. Then a second contact R_{c2} is assumed and followed by the copper resistance R_{Cu}. This repeats inversely until the opposite junction is reached.

Because of the relatively high currents of $4\,kA$ per branch and with the aim to achieve a minimum weight and low surface temperatures, a water cooling system is needed to bear the ohmic heat of the installation. The separate hydraulic branches as seen in Figure 5 do form a hydraulic parallel circuit, which is governed by several thermostatic controlled heater valves (AVTA10-003N1144 [17]) with proportional characteristics (linear transfer function). It is shown in the following Section III that the electric system gives stable performance, although each branch is regulated by its own valve which influences the neighboring branches as well.

A. Electric Design

The present design consists of $n = 5$ branches which contain several components, see Eq. (2). The bulk resistance $R_{Cu,0}$ at room temperature of the copper parts is generally given by

$$R_{Cu,0} = \frac{1}{\sigma_0} \frac{l}{A},$$

(3)

where σ_0 is designated to the materials conductivity. The dimensions are described by l as the length and A as the cross sectional area of the component.

Next to that, the contact resistance

$$R_c \approx \frac{E^* \cdot z}{3.7 \cdot \sigma_0 \cdot F_N}$$

(4)

$$\text{with } E^* = \frac{E}{2 \cdot (1 - \nu_p^2)},$$

(5)

is of importance. Here, the modified E-modul E^* is a function of the Poisson-Number ν_p. Equation (4) gives an approximation for R_c which depends on the force F_N with which the contact surfaces are pressed together and the surface roughness $z \approx 2\,\mu m$ for which a typical value for milling is assumed. However, there is a minimum value which cannot fall below

$$R_{c,min} = \frac{1}{\sigma_0 \cdot D},$$

(6)

for reasons of surface-surface interaction. The parameter D values the characteristic length of the contact which is the width of the radial arm in this context. The necessary contact force $F_N > 1.6\,kN$ for R_{c2} follows from equation (4) and (6). In a rough estimate F_N could be generate sufficiently with an isometric M8 × 1.25 screw which is fastened with a torque of
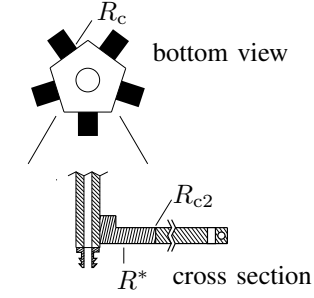
(a) Schematic cross section of the lower junction point. The central rod is water cooled.
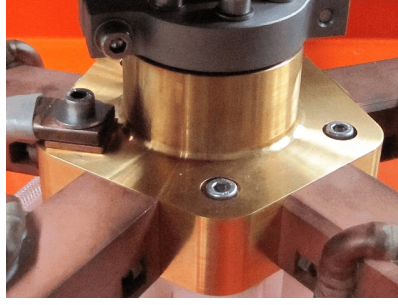
(b) Manufactured part. Coated with gold.
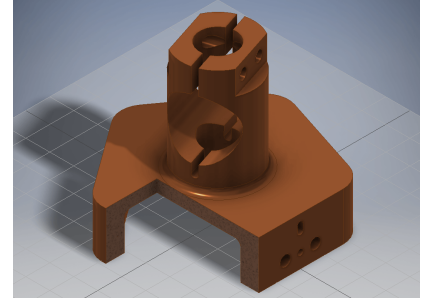
(c) CAD view of upper junction point.

Figure 4: Detailed upper and bottom junction point. In (a) and (b) the central water cooled rod is connected via the junction point to arms. Here bulk resistance R^* and contact resistance R_c are indicated appropriately. The gray jig in (b) ensures sufficient contact pressure to the concentric Morse cone connection. Sub figure (c) illustrates the upper junction point. The sectional view gives insight into the bulk which has a u–shape cross section (both–top and bottom junction).

Table II: Electrical Properties of individual components at $T = 20°C$. l describes the effective length of the component. The contact $R_{c2,min}$ specifies the minimum resistance of an Au-Au system at the junction point into the radial arm. Here D values the characteristic length (width) of the contact.

R_{Cu}	l/m	dimensions	R/µΩ
rod	2.42	$\{d_a, d_i\} = \{30, 10\}$ mm	67.5
arm	0.365	$A = 40 \times 40$ mm^2	4.0
$R_{c2,min}$		$D = 40$ mm	0.55
R^*		complex geometry	≈ 2.47

$M \approx 0.17 \cdot F_N \cdot 8\,\text{mm} > 2.5\,\text{Nm}$ [18, Eq. 8.28]. For further details on contact physics refer the books [19], [20], [21]. In the present design gold coated surfaces form the contacts, so R_c must be determined with respect to $\sigma_{Au,0} = 45.45\,\text{MS/m}$.

The junction resistance R^* is a more complex problem. Here the geometry, symmetry and specific local contact properties influence the current distribution. The geometry of these two junctions is designed as a flat u–shaped pentagonic hollow part. The concentric drilling in conjunction with "thin" wall thickness make a compromise between low resistance and homogeneous current density. Nevertheless, the upper junction point provides some asymmetry, so its resistive contribution varies with the individual contact surface. A stationary simulation with COMSOL Multiphysics 5.2a determines this variation according to Table I.

The fundamental idea of the present design is to balance the current distribution of the five return paths by controlling the temperature of the main return path resistance R_{Cu-rod}. To show the feasibility of this concept, lets estimate the maximum variation of resistance

$$\Delta R = \underbrace{2 \cdot 0.044\,\text{µΩ}}_{\Delta R^*} + \underbrace{4 \cdot 1\,\text{µΩ}}_{\Delta R_c} \tag{7}$$

$$\approx 4.1\,\text{µΩ}$$

along one branch with two junctions and four contacts. The junction point (ΔR^*) and contact (ΔR_c) resistances got a sufficient overrate to respect the uncertainties in the real setup. However, the linear dependence of resistance with temperature

$$R = R_0 \cdot (1 + \alpha \cdot \Delta T) \tag{8}$$

leads to the necessary average temperature change

$$\Delta T = \frac{\Delta R}{\alpha \cdot R_0} \tag{9}$$

$$\approx 16\,\text{K}$$

to cover the required variation of resistance ΔR. Hereby, the reference $R_0 = R_{Cu-rod}$ equals the rod resistance. The specific temperature coefficient is named α. Since the result of Equation (9) gives an average temperature change, one might expect a total temperature difference of $\Delta T = 32\,\text{K}$ between inflow and outflow.

In order to proceed with the thermal design, in the next section the amount of electrical power is needed. The electric behavior is described by a parallel circuit with its total resistance

$$R_{tot} = \left(\sum_{j=1}^{n} \frac{1}{R_{Cu,0} \cdot (1 + \alpha \cdot \Delta T_j)} \right)^{-1} \tag{10}$$

and the individual current

$$I_i = \frac{I_{tot} \cdot R_{tot}}{R_i}$$

$$\approx \frac{I_{tot}}{\sum_{j=1}^{n} \frac{1 + \alpha \Delta T_i}{1 + \alpha \Delta T_j}} \tag{11}$$

on the ith branch. The temperature difference $\Delta T = T_W - 20°C$ is derived from the wall temperature (as bulk temperature) and a reference of 20°C. Equation (10)
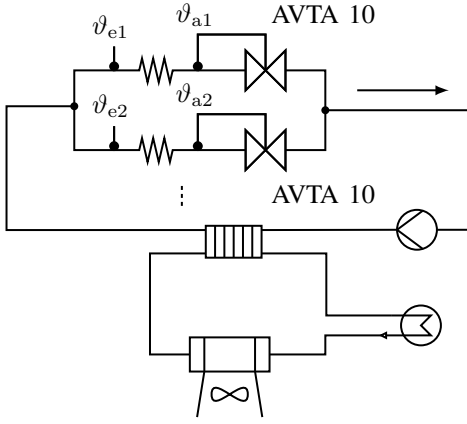
Figure 5: Hydraulic representation of the system. The circuit of the coolant forms a controlled parallel circuit. The valves AVTA 10 open and close according to the outflow temperature ϑ_a. The resistor symbol represents one electric branch, which exhaust heat. The pumps drive the primary (lower) and secondary circle to transport the heat out.

illustrates the non-linear coupling between the individual branches. Now the exhausted ohmic heat

$$
\begin{aligned}
P_{\mathrm{el},i} &= I_i^2 \cdot R_i \\
&= \frac{I_{\mathrm{tot}}^2 \cdot R_{\mathrm{Cu},0}}{\left(\sum_{j=1}^n \frac{1}{1+\alpha \cdot \Delta T_j}\right)^2 \cdot (1 + \alpha \cdot \Delta T_i)}
\end{aligned}
\tag{12}
$$

can be determined from Equations (8), (11) and (10). In the equation above, resistance $R_{\mathrm{Cu},0}$ represents all components in a branch.

B. Thermal Design

To verify whether the proposed water cooling is able to take the heat in general, following thermal design must be carried out.

First of all a pipe flow is considered, which diverts the heat flux

$$
\dot{Q} = \alpha_{\mathrm{th}} \cdot A \cdot \Delta T_{\mathrm{M}}
\tag{13}
$$

form the homogeneously heated wall. The following procedure determines the wall temperature T_{W} as the copper bulk temperature, as suggested in [22]. Remember, since the thermal conductivity of copper is comparably high, the wall temperature T_{W} can be assumed as the bulk temperature.

The thermal coefficient

$$
\alpha_{\mathrm{th}} = \frac{\lambda_{\mathrm{H_2O}} \cdot \mathrm{Nu}}{L}
\tag{14}
$$

as the interaction between pipe flow and wall depends on the thermal conductivity $\lambda_{\mathrm{H_2O}}$ of the coolant, the Nusselt-number

$$
\mathrm{Nu} = 0.012 \cdot \left(\mathrm{Re}^{0.87} - 280\right) \cdot \mathrm{Pr}^{0.4} \cdot \left(1 + \left(\frac{d_\mathrm{i}}{l}\right)^{2/3}\right)
\tag{15}
$$

describing the flow and a characteristic length scale $L = d_\mathrm{i}$ of the system. Where the inner diameter $d_\mathrm{i} = 10\,\mathrm{mm}$ and $l = 2.5\,\mathrm{m}$ define the dimensions of the rod.– Nu is defined for

Table III: Result of the thermal design.

n	$v/(\mathrm{m/s})$	$\dot{Q}_i/\mathrm{kW}$	$T_\mathrm{a}/^\circ\mathrm{C}$	$T_\mathrm{W}/^\circ\mathrm{C}$	$P_{\mathrm{tot}}/\mathrm{kW}$
5	0.848	1.46	25	28	7.3

an intermediate flow range which is present here in ranges of $2300 < \mathrm{Re} < 10^4$ and valid for fluids with $1.5 < \mathrm{Pr} < 500$. Next to that, the average logarithmic temperature difference

$$
\Delta T_{\mathrm{M}} = \frac{T_{\mathrm{out}} - T_{\mathrm{in}}}{\ln \frac{T_{\mathrm{W}} - T_{\mathrm{in}}}{T_{\mathrm{W}} - T_{\mathrm{out}}}}
\tag{16}
$$

is a function of the in- and outflow temperature as well as the mean wall temperature. The Reynolds-Number

$$
\mathrm{Re} = \frac{v \cdot L}{\nu_{\mathrm{H_2O}}}
\tag{17}
$$

scales with flow velocity v. The Prandtl-number Pr as well as Re are calculated from characteristic material parameters depending on the mean fluid temperature T_{M}.

From the calorimetric heat transport balance

$$
P_{\mathrm{el}}\left(T_{\mathrm{W}}\right) = c_{\mathrm{p}} \cdot \rho_{\mathrm{H_2O}} \cdot \frac{\pi}{4} d_\mathrm{i} \cdot v \cdot \left(T_{\mathrm{in}} - T_{\mathrm{out}}\right)
\tag{18}
$$

follows the estimated outflow temperature T_{out}.

Next to that, the wall temperature T_{W} can be determined by an iterative solving procedure, which considers Equations (13)–(18) and the integral power balance

$$
P_{\mathrm{el}}\left(T_{\mathrm{W}}\right) = \dot{Q}_{\mathrm{H_2O}}\left(T_{\mathrm{in}}, T_{\mathrm{out}}, T_{\mathrm{W}}\right)
\tag{19}
$$

as well. Also, this approach takes all thermal material dependencies into account to calculate the estimated values as precise as possible.

The numerical results listed in Table III prove that the suggested water cooling system (see Table VIII) is sufficient to take the ohmic heat under all circumstances. Therefore it is important to see that the outflow temperature T_{out} increases only $5\,\mathrm{K}$ at maximum flow speed, which gives a certain reserve for controlling. In consequence, the necessary (controlled) throttle valve would be able to rise the temperature above the required ΔT to control the electrical current accordingly.

III. PROOF OF CONCEPT

The general idea of the present temperature controlled circuit is to equalize the current by minimizing the empirical standardized deviation

$$
s = \sqrt{\frac{1}{n-1} \sum_i \left(\frac{I_{\mathrm{tot}}}{n} - I_i\right)^2} \to \min,
\tag{20}
$$

$$
\text{with } I_{\mathrm{tot}} = \sum_i I_i = \text{const.}
\tag{21}
$$

and keeping the total current I_{tot} constant at the same moment. With respect to the denominator of Equation (12), it becomes clear that the ith branch in a parallel circuit of heated conductor is influenced by the temperature distribution along all other branches. In other words, the specific heat power $P_{\mathrm{el},i}$ is a result of all temperatures T_j which determine the current distribution

Table IV: First case study with $R_n = $ const.. As initial condition the temperatures are random distributed.

		Temperatures in °C				
i	s_I/A	$T_\mathrm{out,1}$	$T_\mathrm{out,2}$	$T_\mathrm{out,3}$	$T_\mathrm{out,4}$	$T_\mathrm{out,5}$
1	336	5.7	26.7	62.9	-9.78	104
2	10^{-4}	37.2	37.2	37.1	37.22	37.1
3	10^{-10}			37.2		

Table V: Second case study with $R_n \in \{69.58, 71.51, 68.12, 69.84, 67.3\}\,\mu\Omega$. As initial condition the temperatures are random distributed.

		Temperatures in °C				
i	s_I/A	$T_\mathrm{out,1}$	$T_\mathrm{out,2}$	$T_\mathrm{out,3}$	$T_\mathrm{out,4}$	$T_\mathrm{out,5}$
1	104	27.2	23.2	21.9	14.1	20.5
2	93.8	39.74	39.72	39.76	39.76	39.78
5	39.7	38.3	30.0	44.8	37.1	48.6
10	9.4	37.3	24.5	47.6	35.6	53.5
20	0.54	37.0	22.8	48.3	35.0	54.9
50	10^{-4}	37.0	22.7	48.3	35.0	54.9

in the system. However, it must be proved that an electric and hydraulic coupled circuit gives stable performance.

Constant temperatures can be achieved with simple thermostatic operated valves like the AVTA10 with absorption charge [17]. An estimate of its linear transfer function

$$T_\mathrm{out} = k \cdot \underbrace{I^2 \cdot R}_{P} + T_0 \qquad (22)$$

$$\text{with} \qquad k = 5.96 \cdot 10^{-4}\,\mathrm{K/W},$$
$$\text{and} \qquad T_0 = 39.1°\mathrm{C}$$

in the present application was determined experimentally as shown in Appendix A.

Suppose that the mean temperature difference

$$\Delta T_i = \frac{1}{2}\left(T_\mathrm{out}\left(I_i\right) + T_\mathrm{in}\right) - 20°\mathrm{C} \qquad (23)$$

$$= \frac{k \cdot I^2 \cdot R}{2} + \underbrace{\frac{T_0 + T_\mathrm{in}}{2} - 20°\mathrm{C}}_{T_\mathrm{O}} \qquad (24)$$

is a linear function of the electric heat power (see Eq. (22)), it now becomes possible to close the equation loop with (12). Putting everything together, yields the recursive form

$$\Delta T_i(\delta) = \frac{\frac{1}{2}k \cdot I_\mathrm{tot}^2 \cdot R_{\mathrm{Cu},0}}{\left(\sum_{j=1}^{n}\frac{1}{1+\alpha \cdot \Delta T_j(\delta-1)}\right)^2 \cdot (1+\alpha \cdot \Delta T_i(\delta-1))} + T_\mathrm{O}, \qquad (25)$$

which cannot be reduced further because of the quadratic denominator. The discrete time step is denoted with δ.

Now, an iterative loop calculates Equation (25) and optimizes T_O in a way that Equations (20) and (21) stay valid. The latter considers the different set points of operation to compensate different branch resistances and carries out a numerical calibration of the system. This method proves that there is a possible calibrated set point which remains stable.

The first case study is given in Table IV and shows that for equal branch resistance R_n the temperature profile converges very fast to a constant and equal distribution. Although a subsequent branch is influenced electrically and hydraulically by all other sections, the system behaves like expected and provides stable performance.

The second case study extends the problem to differing R_n, according to Table V. Here the outflow temperature is balanced in a way that the variations in R_n are balanced by (numerical) calibration. This is done by setting T_0 from Equation (22) appropriately. Comparing the total number of iterations i the full design problem takes much longer to converge indicating that the calibration of a real system could be challenging.

However, it could be proved even for random initial distribution of $R_n = (69.3 \pm 2.1)\,\mu\Omega$, it is possible to equalize the branch resistances therebybalancing all currents to reach the design goal of minimal current deviation.

IV. EXPERIMENTAL PROOF OF CONCEPT

To quantify the current distribution along all rods, five ironless clamp-on current probes of the type CPCO-4000-77-SE [23] ($\pm 4\,\mathrm{kA}$ measurement range) with less than 1% relative accuracy are used. Hereby, the special coreless design of this recent sensor eliminates the influence of external stray fields, which must be considered with other sensors. The limiting parameter for common sensor applications would be the low distance of about $0.5\,\mathrm{m}$ to the next return path or the central rod. In addition to that, the magnetic field homogeneity is not disturbed either by any iron, coming along with other sensor types for such current scales.

Figure 6 displays the results of a commissioning run. Here the total current was set to $I_\mathrm{tot} = 10.2\,\mathrm{kA}$. In the first few seconds the initial switch-on event takes place. Due to the low sampling frequency of $f_\mathrm{s} = 1\,\mathrm{Hz}$ the standard deviation in panel (c) jitters a lot in the beginning. Until approximately $300\,\mathrm{s}$ the valves remain closed so the initial accuracy of the system ($s \approx 10\,\mathrm{A}$) can be observed. During this first phase the copper heats up, so that all parameters (resistivity, contact pressure, ect.) start to change smoothly. This results in a decreasing current deviation till valve number two starts to act which can be seen from now on as the constant temperature T_2. At the same time the current deviation s changes massively until the moment when all valves are throttling the flow. Because the utilized gas charge controlled valves act rather slow the system takes about $10\,\mathrm{min}$ to relax. With respect to the rather large hydraulic response time the change of resistance is direct coupled to the temperature variation. In contrast to that the current balance remains a result of the parallel circuit of the hydraulic and electric system (see Fig. 3) which effects the swing at $5\ldots 8\,\mathrm{min}$ in Figure 6b. After this initial relaxing phase all valves act and the standard current deviation falls below $s < 6.7\,\mathrm{A}$, indicating the accuracy limit of one single sensor. The remaining oscillations in the graph are related to the characteristic frequencies of the $300\,\mathrm{kW}$ cooling system in the lab.
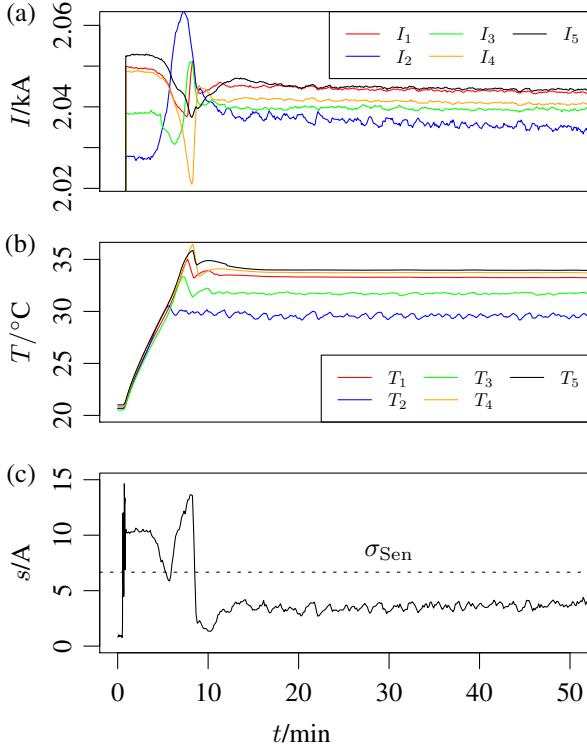
Figure 6: Results of a first commissioning run. In (a) the individual currents are displayed. Panel (b) provides the related outflow temperatures and (c) depict a time series of empirical standard deviation calculated from each time step in (a). With a total current of $I_{\text{tot}} = 10.2\,\text{kA}$ the calibrated system reaches an imbalance of less than $\Delta I < 26.25\,\text{A}$ (corresponds to $\pm 6\sigma$-range) over all five return paths, which is less than 0.26% in terms of relative error compared to the total current.

Assuming a normal distributed process with $I_n = 2.04\,\text{kA} \pm \Delta I$, the maximum expected current deviation along all five branches can be calculated to

$$\Delta I_{\text{max}} = t_{1-\alpha,n} \cdot s \tag{26}$$
$$\approx 26.25\,\text{A}$$

which estimates a $\pm 6\sigma$ confidence range with Student's t-distribution with $n = 5$ degrees of freedom and $1 - \alpha$ appropriate to the allowed variation. Compared to the total current the relative distribution error is about 0.26%.

The maximum deviation of the sensor system consisting of five devices

$$\Delta I_{\text{Sen}} < \frac{t_{1-\alpha,n}}{\sqrt{n}} \cdot \sigma_{\text{Sen}} \tag{27}$$
$$< 22.3\,\text{A}$$
$$\text{with } \sigma_{\text{Sen}} = 1\% \cdot 4\,\text{kA} \cdot \frac{1}{6}$$
$$\approx 6.7\,\text{A}$$

can be estimated under the assumption of equal current distribution in the system. The degree of freedom remains $n = 5$ because the mean value is assumed to be known and equal on all sensors. Last, the sensor accuracy of 1% might

cover a $\pm 6\sigma$ range, too. In the test run ΔI_{Sen} is close to ΔI_{max} indicating that an optimum calibration is reached.

The remaining drift of I_n and σ is mainly caused by the missing thermal insulation driving free convection along the vertical rods. Remember Equation (25), here all possible heat flux contribute to the temperature rise of the coolant, whereas a free convection or radiation would introduce an additional leakage term. The suggested rod insulation has already been installedto stabilize the system with respect to the heat flux which entirely passes through the sensor of heat valve now.

The whole system was calibrated as seen in Figure 6 for a mid amperage of about $10\,\text{kA}$. It turns out that the highly linear nature of the design problem gives stable and accurate performance up to the maximum system current of $20\,\text{kA}$ with a relative current deviation of about 0.30%.

V. CONCLUSION

A quasi coaxial setup consisting of a central rod and five symmetric return paths is designed in the present high current application. Hereby, standard thermostatic controlled heater valves balance the current in the system, achieving an equal distribution along the separate branches. The detailed analysis of the involved electric and hydraulic elements showed that the approach to utilize the thermal dependence of resistivity is promising. The numerical investigation on this supports the idea that a proportional regulated valve is sufficient to keep the branch resistance constant even in a non-linear coupled system. The present design also shows that with very simple and affordable components (current sensor and AVTA valve, each $\approx 150\,\text{€}$) a balanced and precise high current distributor can be built. One of the goals is the usage of electronic free components which provide a robust and easy to maintain system.

After calibration, the real installation gives a predictable stable performance. The measured deviation in current distribution is about 0.26% and therefore in the same order of magnitude compared to the accuracy of the current measurement system involving five sensors. Subsequently, the system performance is maximized to the measuring range limits of the sensor system with a relative full scale error of 0.22%, which is more than one order of magnitude better than the desired design goal of five percent.

APPENDIX A
CHARACTERISTICS OF THE HEAT VALVE

In preparation of the proof of concept it was necessary to obtain the transfer functions

$$T_{\text{out}} = f(I) \tag{28}$$
$$\text{and } T_{\text{out}} = f(P) \tag{29}$$

of the utilized valve (Danfoss AVTA10-003N1144 with adsorption charge [17]) in conjunction with the $2.5\,\mathrm{m}$ long copper rod and a single line coolant supply. The main reason for the experiments on the valve was the lack of information about the control loop characteristics of the device.

The setup is very simple, a variable current $0\ldots20\,\mathrm{kA}$ is introduced to a copper rod with $d_\mathrm{i} = 10\,\mathrm{mm}$, $d_\mathrm{a} = 30\,\mathrm{mm}$ and a maximal flow speed of $v \approx 0.85\,\mathrm{m/s}$ at $\Delta p = 5.5\,\mathrm{bar}$ pressure difference. A PT100 element measures the temperature at the point of outflow. The desired valve is supposed to keep the outflow temperature $T_\mathrm{out} \approx 40°\mathrm{C}$ up to a certain level constant. Because of the proportional behavior a temperature dependent deviation from the set point can be expected.

The result of the experimental investigation can be found in Figure 7. Here the transfer function can be split in three sections –a sub-critical, normal operation and super-critical operating area. In the normal operation range from $5\,\mathrm{kA} < I < 11\,\mathrm{kA}$ the linearized transfer functions

$$T_\mathrm{out} = 6.78 \cdot 10^{-4}\,\frac{\mathrm{K}}{\mathrm{A}} \cdot I + 36.4°\mathrm{C} \qquad (30)$$

$$\text{and} \qquad = 5.94 \cdot 10^{-4}\,\frac{\mathrm{K}}{\mathrm{W}} \cdot P + 39.1°\mathrm{C} \qquad (31)$$

can be found.

In the sub-critical regime too many of CO_2 is released out of the active carbon filling in the thermostatic sensor, as a consequence the valve opens too much. In contrast to that, the super critical right side of the diagram indicates, that the valve is opened completely. The regulation reserve is depleted in this case.

To cover the region from $0 < I_i < 4\,\mathrm{kA}$ in the final design a set point with lower T_out value must be used. Refer to Figure *6*, where $T_\mathrm{out} < 35°\mathrm{C}$ was set. Also the reduced flow rate in the hydraulic parallel circuit will shift the diagram as well.
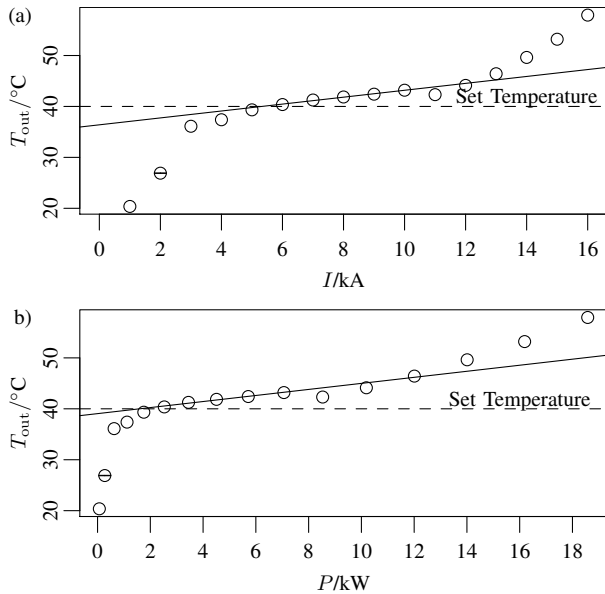

Figure 7: Control loop characteristics of AVTA 10. The desired set temperature is $T_\mathrm{set} = 40°\mathrm{C}$.

APPENDIX B
SIMULATION OF THE UPPER JUNCTION

The simulation of the upper junction point was carried out with the 'mef' module in COMSOL. The result can be seen below. Here it becomes clear, that a certain asymmetry governs the system since the outflow (periphery surfaces 1–5) is grounded and the horizontal rod connection is modeled as 'contact'. The latter leads to a realistic concentration of current density at the bottom side of the contact. The resulting resistances are listed in Table I.
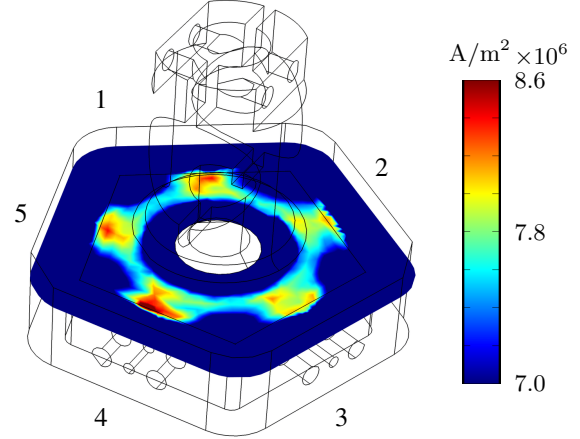

Figure 8: Simulation of the current density in the upper junction at $20\,\mathrm{kA}$ of total current. It clearly indicates an asymmetry and therefore different effective resistances. The numbers indicate the count of the surfaces where the current exits the bulk.

APPENDIX C
MATERIAL AND MODEL PARAMETERS

Table VI: Properties of copper Cu-ETP [24], [25] at room temperature $T_0 = 20°\mathrm{C}$

	Value	Comment
ρ_0	$8930\,\mathrm{kg/m^3}$	
c_p	$386\,\mathrm{J/(kg \cdot K)}$	
λ_0	$394\,\mathrm{W/(m \cdot K)}$	
σ_0	$57\,\mathrm{m/\left(\Omega \cdot mm^2\right)}$	el. cond.
α	$3.9 \cdot 10^{-3}\,\mathrm{K^{-1}}$	th. coeff. for resistivity
E	$130\,\mathrm{GPa}$	E-modul
ν_p	$0.34\ldots0.35$	Poisson-num.

Table VII: Properties of water [22] at a Temperature of $T = 40°\mathrm{C}$

	Value	Comment
$\nu_\mathrm{H_2O}$	$0.66 \cdot 10^{-6}\,\mathrm{m^2/s}$	kinematic viscosity
$\rho_\mathrm{H_2O}$	$992\,\mathrm{kg/m^3}$	
$\mathrm{Pr}_\mathrm{H_2O}$	4.3	Prandtl-Number
$\lambda_\mathrm{H_2O}$	$631 \cdot 10^{-3}\,\mathrm{W/(m \cdot K)}$	thermal conductivity

Table VIII: Design and model parameters. * The value for the flow velocity is an approximated value in a single line from a measurement in the lab. Here we find a roughly $10\,\mathrm{m}$ long hydraulic system consisting of hoses, corners and valves.

	Value	Description
n	5	no. of branches
I_tot	$20\,\mathrm{kA}$	total current
d_i	$10\,\mathrm{mm}$	inner diameter
d_a	$30\,\mathrm{mm}$	outer diameter
l	$2.5\,\mathrm{m}$	hydraulic length
h	$2.42\,\mathrm{m}$	electric length
v	$0.85\,\mathrm{m/s}$	flow velocity*
Δp	$5.5\,\mathrm{bar}$	diff. pressure
T_in	$20°\mathrm{C}$	inflow temp.

REFERENCES

[1] A. H. R. Mallock, "Determination of the viscosity of water," *Proceedings of the Royal Society of London*, vol. 45, no. 273-279, pp. 126–132, 1888.

[2] ——, "Experiments on fluid viscosity," *Philosophical Transactions of the Royal Society of London. Series A, Containing Papers of a Mathematical or Physical Character*, vol. 187, pp. 41–56, 1896.

[3] M. F. A. Couette, "Etudes sur le frottement des liquides," Dissertation, Gauthier-Villars, 1890.

[4] L. Rayleigh, "On the dynamics of revolving fluids," *Proceedings of the Royal Society of London. Series A*, vol. 93, no. 648, pp. 148–154, 1917.

[5] G. I. Taylor, "Stability of a viscous liquid contained between two rotating cylinders," *Philosophical Transactions of the Royal Society of London. Series A, Containing Papers of a Mathematical or Physical Character*, vol. 223, pp. 289–343, 1923.

[6] D. H. Michael, "The stability of an incompressible electrically conducting fluid rotating about an axis when current flows parallel to the axis," *Mathematika*, vol. 1, no. 01, pp. 45–50, Jun. 1954.

[7] S. Chandrasekhar, "The stability of viscous flow between rotating cylinders in the presence of a magnetic field," *Proceedings of the Royal Society of London A: Mathematical, Physical and Engineering Sciences*, vol. 216, no. 1126, pp. 293–309, 1953.

[8] E. P. Velikhov, "Stability of an ideally conducting liquid flowing between rotating cylinders in a magnetic field," *Soviet physics / JETP*, vol. 36, pp. 995–998, 1959.

[9] S. A. Balbus and J. F. Hawley, "A powerful local shear instability in weakly magnetized disks. I-Linear analysis. II-Nonlinear evolution," *The Astrophysical Journal*, vol. 376, pp. 214–233, 1991.

[10] R. Hollerbach and G. Rüdiger, "New Type of Magnetorotational Instability in Cylindrical Taylor-Couette Flow," *Physical Review Letters*, vol. 95, no. 12, Sep. 2005.

[11] G. Rüdiger and M. Schultz, "The Magnetorotational Instability of MHD Taylor-Couette Flows," *Magnetohydrodynamics*, vol. 42, no. 2-3, pp. 3–11, 2006.

[12] F. Stefani, T. Gundrum, G. Gerbeth, G. Rüdiger, M. Schultz, J. Szklarski, and R. Hollerbach, "Experimental evidence for magnetorotational instability in a helical magnetic field," *Physical Review Letters*, vol. 97, no. 18, Nov. 2006.

[13] M. Seilmayer, V. Galindo, G. Gerbeth, T. Gundrum, F. Stefani, M. Gellert, G. Rüdiger, M. Schultz, and R. Hollerbach, "Experimental Evidence for Nonaxisymmetric Magnetorotational Instability in a Rotating Liquid Metal Exposed to an Azimuthal Magnetic Field," *Physical Review Letters*, vol. 113, no. 2, p. 024505, Jul. 2014.

[14] M. Seilmayer, T. Gundrum, and F. Stefani, "Noise reduction of ultrasonic Doppler velocimetry in liquid metal experiments with high magnetic fields," *Flow Measurement and Instrumentation*, vol. 48, pp. 74–80, Apr. 2016.

[15] Fuji Electric, "1MBI3600U4D-120 – IGBT Module (U series)," Fuji Denki Holdings, Shinagawa, Japan, Datasheet, 2013.

[16] V. K. Singh and E. Anil Kumar, "Measurement and analysis of adsorption isotherms of CO2 on activated carbon," *Applied Thermal Engineering*, vol. 97, pp. 77–86, Mar. 2016.

[17] "Danfoss AVTA-Ventile," Nordborg, Denmark, Datasheet DKACV.PD.500.A4.03, 2002.

[18] H. Wittel, D. Muhs, D. Jannasch, and J. Voßiek, *Roloff/Matek Maschinenelemente: Tabellenbuch*, 19th ed. Wiesbaden: Vieweg + Teubner, 2009.

[19] R. Holm, *Electric Contacts Handbook*, 3rd ed. Heidelberg: Springer-Verlag, 1958.

[20] E. Vinaricky and A. Keil, Eds., *Elektrische Kontakte, Werkstoffe und Anwendungen: Grundlagen, Technologien, Prüfverfahren*, 2nd ed. Berlin: Springer, 2002.

[21] V. L. Popov, *Kontaktmechanik und Reibung: ein Lehr- und Anwendungsbuch von der Nanotribologie bis zur numerischen Simulation*. Berlin: Springer, 2009.

[22] Verein Deutscher Ingenieure, *VDI-Wärmeatlas*, 11th ed. Berlin, Heidelberg: Springer Vieweg, 2013.

[23] GMW Associates, "CPCO Series DC-AC Current Probe, Clamp On 77mm, ±4000A," San Carlos, USA, Datasheet, Oct. 2015.

[24] H. Rohlfing, *Tabellenbuch für Elektrotechnik*. Bonn: Dümmler, 1975.

[25] Deutsches Kupfer Institut, "Cu-ETP – DKI Werkstoff-Datenblätter," Deutsches Kupfer Institut, Düsseldorf, Datasheet, 2015.

Martin Seilmayer was born in Dresden, Germany in 1985. He received his diploma in 2010 in electrical engineering at the Technische Universität Dresden. Up to now he works at Helmholtz-Zentrum Dresden-Rossendorf in the Department of Magnetohydrodynamics. There, he finished his PhD in 2015 on "Studies on magnetohydrodynamic instabilities in liquid metal flows". Two of the key topics of his work are signal processing and pattern recognition.

Nico Krauter was born in Dresden, Germany in 1989. He received his diploma in 2014 in electrical engineering at the Technische Universität Dresden. Up to now he works at Helmholtz-Zentrum Dresden-Rossendorf in the Department of Magnetohydrodynamics. There, he is working on his PhD since 2015, developing and investigating inductive velocity sensors for liquid metal flows as well as performing numerical simulations of electric and magnetic fields.